Pergamon

Geochimica et Cosmochimica Acta, Vol. 60, No. 18, pp. 3471–3485, 1996

0016-7037/96 $15.00 + .00

PII S0016-7037(96)00178-0

Thermodynamic properties and isotopic fractionation of calcite from vibrational spectroscopy of ^{18}O-substituted calcite

PHILIPPE GILLET,[1] PAUL MCMILLAN,[2] JACQUES SCHOTT,[3] JAMES BADRO,[1] and ANDRZEJ GRZECHNIK[2]

[1]Institut Universitaire de France, Laboratoire de Sciences de la Terre, Ecole Normale Supérieure des Sciences, URA 726, CNRS, 46 allée d'Italie, 69365 Lyon Cedex 07, France
[2]Materials Research Group in High Pressure Synthesis, Department of Chemistry and Biochemistry, Arizona State University, Tempe, Arizona 85287, USA
[3]Laboratoire de Mécanismes de Transfert en Géologie, URA 67 CNRS, Université de Toulouse 3, 38 rue des Trente-six Ponts, 31400 Toulouse Cedex, France

(*Received September* 1, 1995; *accepted in revised form May* 20, 1996)

Abstract—The infrared and Raman spectra of $CaCO_3$ calcite substituted with 80% ^{18}O have been recorded. A detailed mode assignment is proposed for all the observed bands, including combinations and overtones. These data are used to propose a simplified model of the vibrational density of states (VDOS) from which the specific heat, the entropy, and the high-temperature equation of state are calculated. Excellent agreement between calculated and measured values of the thermodynamic properties is obtained when measured vibrational mode anharmonicity is included in the calculations. The model can be used to infer the properties of calcite at high pressures ($\leq$3 GPa) and temperatures ($\leq$1200 K). The observed frequency shifts induced by ^{18}O substitution in both IR and Raman spectra are used to construct the VDOS of $CaC^{18}O_3$ calcite. The reduced partition function of calcite is then calculated and the effects of anharmonicity are discussed. Finally the effect of pressure on the reduced partition function is calculated and is shown to be appreciable even at high temperatures.

1. INTRODUCTION

Carbonates form a major class of rock-forming minerals in both low and high temperature and pressure environments. In this paper we calculate the thermodynamic properties of calcite using vibrational modelling over the temperature and pressure range of 300–1200 K and 0–3 GPa, respectively. There have been numerous previous studies devoted to the modelling of these properties using either lattice dynamics models (Plihal, 1973; Catti et al., 1993; Dove et al., 1992) or vibrational modelling (Salje and Viswanathan, 1976; Kieffer, 1979). However, all of the proposed calculations have been performed under harmonic or quasi-harmonic assumptions and, as a consequence, they do not reproduce accurately the specific heat and entropy of calcite, at temperatures above 700 K. We have, therefore, chosen to calculate the specific heat and entropy of carbonates using an anharmonic vibrational model which has been successfully tested on other minerals (Gillet et al., 1989, 1991, 1992; Fiquet et al., 1992; Reynard and Guyot, 1994; Guyot et al., 1996).

We have prepared samples of calcite ($CaCO_3$) highly enriched with ^{18}O, and have measured their infrared and Raman vibrational spectra. These data are combined with our previous measurements of vibrational mode anharmonicity in calcite (Gillet et al., 1993) to provide a well-constrained calculation of entropy, specific heat, and volume at high temperature and pressure as well as of the isotope fractionation factor. This approach is a standard practice for over 50 years (e.g., Herzberg, 1945) and has been popularized by Kieffer (1979, 1982) in Earth's Sciences, with highly encouraging results, but has been limited by the lack of vibrational data for isotopically substituted minerals.

2. EXPERIMENTAL

2.1. Sample Synthesis

$CaC^{18}O_3$ calcite was synthesized in a two step process. In a first experiment an oxygen 18-rich calcite was precipitated at 295 K from a 1.12 m $NaHCO_3$ solution via stoichiometric addition of solid Prolabo Normapur $CaCl_2$ (5 g of $NaHCO_3$ solution + 0.66 g $CaCl_2$). The $NaHCO_3$-^{18}O enriched solution was prepared by dissolving in an air-free syringe 0.5 g $NaHCO_3$ (Prolabo Normapur) in 5 g $H_2{}^{18}O$ (>95% $H_2{}^{18}O$, EurisoTop). Using the equation given by Usdowski et al. (1991), it was calculated that 9000 min. were necessary for HCO_3-(aq) to reach isotopic equilibrium. Thus, the exchange reaction was allowed to proceed for one week. All these reactions were carried out under nitrogen pressure to avoid any exchange between aqueous and gaseous H_2O, CO_2, and O_2. Raman spectra recorded on this precipitated calcite showed that $C^{16}O_3$ groups largely dominated the $C^{18}O_3$ groups. No explanation was found for the low ^{18}O content of these samples. In a second step, this precipitated calcite and 0.5 g of $H_2{}^{18}O$ were allowed to react at 713 K and 0.1 GPa during three weeks in a gold capsule placed in a cold-seal autoclave. About 80% of the total oxygen was ^{18}O and this sample was subsequently used in the present study.

2.2. Raman Spectroscopy

A Dilor® XY double subtractive spectrograph with premonochromator (1800 g/mm holographic gratings), equipped with confocal optics before the spectrometer entrance, and a nitrogen-cooled EGG® CCD detector are used. A microscope is used to focus the excitation laser beam (488 nm or 514 nm exciting line of a Spectra Physics® Ar^+ laser) on the sample and to collect the Raman signal in the backscattered direction. The presence of the confocal pinhole before the spectrometer entrance ensures a sampling of a 2–3 μm sized zone. Accumulations of 120–300 seconds have been made.

2.3. Infrared Spectroscopy

Infrared absorption measurements were carried out using a Bio-Rad Digilab FTS-40 interferometer. Finely powdered samples were

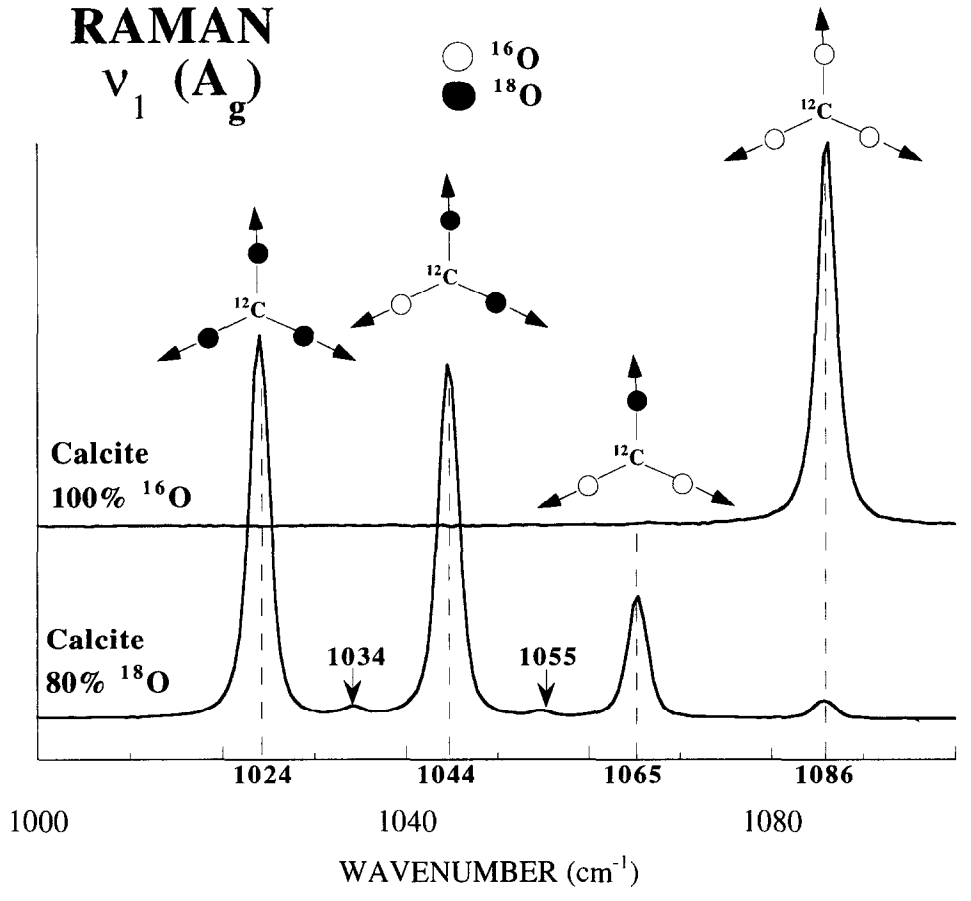

FIG. 1. Raman spectra and atomic motions of the ν_1 vibration of the CO_3^{2-} group in both $CaC^{16}O_3$ and $CaC^{18}O_3$.

pressed into a polycrystalline film between two Type IIa diamonds selected for infrared transmission studies. The top diamond was removed, and the infrared spectrum of the calcite sample was recorded at ambient conditions. Mid-IR spectra were obtained using a Globar source, KBr beamsplitter, and HgCdTe detector. Far-IR spectroscopy was carried out with a Hg lamp source, Mylar beamsplitter, and DTGS detector. Care was taken to completely purge the instrument with dry air before the far-IR experiment. Resolution in both regions of the spectrm was on the order of 2–4 cm^{-1}.

3. INFRARED AND RAMAN SPECTROSCOPIC DATA

The Raman spectra are dominated by the ν_1 symmetric stretching vibration in the 1000–1100 cm^{-1} region (Fig. 1). The unsubstituted sample ($CaC^{16}O_3$) shows a single peak at 1086 cm^{-1} (White, 1974; Gillet et al., 1993) The first synthesis attempt resulted in only a slightly-^{18}O-substituted sample. This sample showed an additional weak peak at 1065 cm^{-1}, due to singly-substituted carbonate groups ($C^{16}O_2{}^{18}O$), in agreement with the previous study of Cloots (1991) (the expected vibrational isotope shift for a single oxygen atom substitution within the CO_3^{2-} group is $\nu_1/\nu_1^* = \sqrt{m_{16_O}/m_{18_O}}$ = 0.9798: theoretical ν_1 for $CaC^{16}O_2{}^{18}O$ = 1064 cm^{-1}). The sample substituted with approximately 80% ^{18}O shows a considerably different pattern in the region of the ν_1 vibration (Fig. 1). There are two strong peaks at 1024 and 1044 cm^{-1}, and weaker peaks at 1065 and 1086.8 cm^{-1}. These correspond to the ν_1 symmetric stretching vibrations of CO_3^{2-} groups substituted with 3, 2, 1, and 0 ^{18}O atoms, respectively, in agreement with the calculated isotopic frequency ratios ($\nu_1/\nu_1^* = \sqrt{m_{16_O}/m_{18_O}}$ = 0.9428, 0.9608, and 0.9798, respectively). The relative intensity ratios of these peaks are related to the amount of ^{18}O present in the sample. The proportion of the various CO_3^{2-} groups depends on the available number of ^{18}O atoms. A simple statistical denumbering shows that the 4:1 intensity ratio observed between the ν_1 mode corresponding to $C^{16}O_3^{2-}$ at 1086 cm^{-1} and the ν_1 mode corresponding to $C^{18}O_3^{2-}$ at 1024 cm^{-1} agrees with a degree of partial substitution on the order of 80%. It is of interest that the centre of symmetry in the calcite structure lies between adjacent carbonate groups, so that the partially substituted groups $C^{16}O_2{}^{18}O$ and $C^{16}O^{18}O_2$ have the possibility of forming locally noncentrosymmetric structures, depending on the ordering scheme of oxygen isotopes in adjacent groups. This explains the appearance of the two weak features in the infrared spectrum at 1045 and 1066 cm^{-1}, corresponding to the ν_1 vibrations of partially substituted groups rendered IR-active by the disappearance of the inversion centre, and relaxation of the g ≠ u selection rule (Fig. 2).

It is also of interest that very weak satellite peaks appear

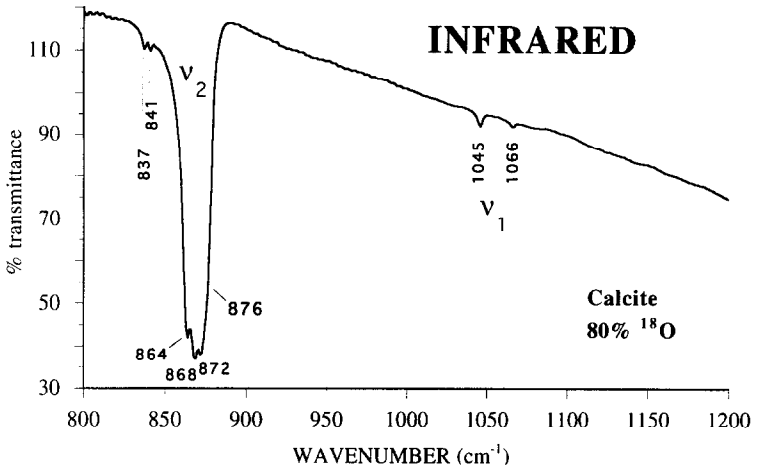

FIG. 2. Infrared spectrum of the ν_1 and ν_2 vibrations of the CO_3^{2-} in ^{18}O substituted calcite.

in the Raman spectrum, evenly spaced (Δ = 10.5 cm^{-1}) between the ν_1 vibrations of the partially substituted isotopic samples (Fig. 1). These have no obvious origin in a mass effect associated with isotopic substitution, and are absent in the spectrum of the unsubstituted ($C^{16}O_3$) sample. We propose that these weak satellites arise because of interference between the Raman-scattered photons emitted from adjacent partially-substituted CO_3^{2-} sites, to give photons at wavenumber ϕ_0-(ϕ_1 + ϕ_2)/2 (ϕ_0, ϕ_1 and ϕ_2 refer to the incident photon, and Raman-scattered phonons from different sites, respectively). This type of mixing might be expected in a crystal structure with large electro- and piezo-optic coupling associated with the strongly Raman-active ν_1 mode, especially in the absence of a centre of symmetry around the partly substituted sites. This behaviour could even suggest that partly ^{18}O-substituted calcite might find application as a photorefractive material, or be useful for frequency doubling of visible light.

The next region of the spectrum which is most easily analyzed is the ν_4 bending region, at around 670–710 cm^{-1} (Fig. 3) This vibration would give rise to infrared- (E_u) and Raman- (E_g) active components, for completely substituted calcite structures ($C^{16}O_3$ and $C^{18}O_3$). If the isolated carbonate groups are considered, as is necessary for the case of the present partially substituted structure, it is more appropriate to use the site group symmetry D_3, with symmetry species E for the fully substituted groups within the partially substituted structure. For pure $CaC^{16}O_3$, this vibration gives rise to the modes at 709 (Raman) and 711 cm^{-1} (IR). The near-coincidence of the IR and Raman frequencies reveals that there is little or no vibrational (Davydov) coupling between the carbonate groups for this vibration (White, 1974). The same is true for the fully substituted group ($C^{18}O_3$), which gives rise to the IR and Raman peaks at 674 and 673.5 cm^{-1}, respectively (Fig. 3). The intermediate substitutions give rise to two pairs of doublets, because the doubly degenerate mode is split into two components by the partial isotopic substitution. The point group for the partially substituted carbonate group becomes C_{2v} instead of D_{3h}. For $C^{16}O_2{}^{18}O$, the higher frequency component involving motion of the lighter isotope will have B_2 symmetry within this point group and the lower frequency component is A_1, whereas for the other isotopic substitution pattern ($C^{16}O^{18}O_2$) the mode symmetry assignment is reversed (Fig. 3). These give rise to the Raman- and IR-active modes at 699 and 694 cm^{-1}, and 689 and 681 cm^{-1}, respectively (Fig. 3).

In the region of the ν_3 vibration (doubly degenerate (E_g) Raman mode at 1432 cm^{-1} for unsubstituted calcite), the isotopically substituted sample shows a single, broad peak with its maximum at 1418 cm^{-1} (Fig. 4). This peak is asymmetric to its high frequency side, consistent with the partially substituted sample. The infrared band is characterized by a large TO-LO splitting (E_u^T 1407 cm^{-1}; E_u^L 1549 cm^{-1} for unsubstituted calcite; White, 1974), so that no reliable information on the resonant frequencies of the isotopically substituted species can be obtained from this powder measurement (Fig. 5). It is likely from the Raman spectrum that these would be unresolved, in any case. Also visible in Fig. 4 are the first overtones from the ν_2 deformation vibration of the isotopically substituted carbonate groups, near 1730 cm^{-1}. For unsubstituted calcite, one component of the fundamental vibration has A_{2g} symmetry and is Raman inactive. A recent Raman spectroscopic study of $CaMg(CO_3)_2$ (dolomite) suggests that this vibration may occur near 880 cm^{-1} in calcite (Gillet et al., 1993). The other fundamental component has symmetry A_{2u}, and is observed at 872 cm^{-1} (LO at 890 cm^{-1}) in the infrared spectrum. Both $2\nu_2$ combinations have A_{1g} symmetry, and give rise to a weak band observed in Raman spectra of unsubstituted calcite at 1748 cm^{-1} (Kraft et al., 1991; Gillet et al., 1993). The $2\nu_2$ vibration of the fully ^{18}O substituted species occurs at 1727 cm^{-1} in the Raman spectrum, whereas partially substituted species give rise to peaks at 1735 and 1742 cm^{-1} (Fig. 4).

The infrared active ν_2 fundamental is easily observed near 870 cm^{-1} (Fig. 5), and its fine structure for the partially substituted sample is discerned in Fig. 2. The three maxima at 864, 868, and 872 cm^{-1} can be assigned to the ν_2 vibrations of the partially substituted samples with $C^{18}O_3$, $C^{16}O^{18}O_2$,

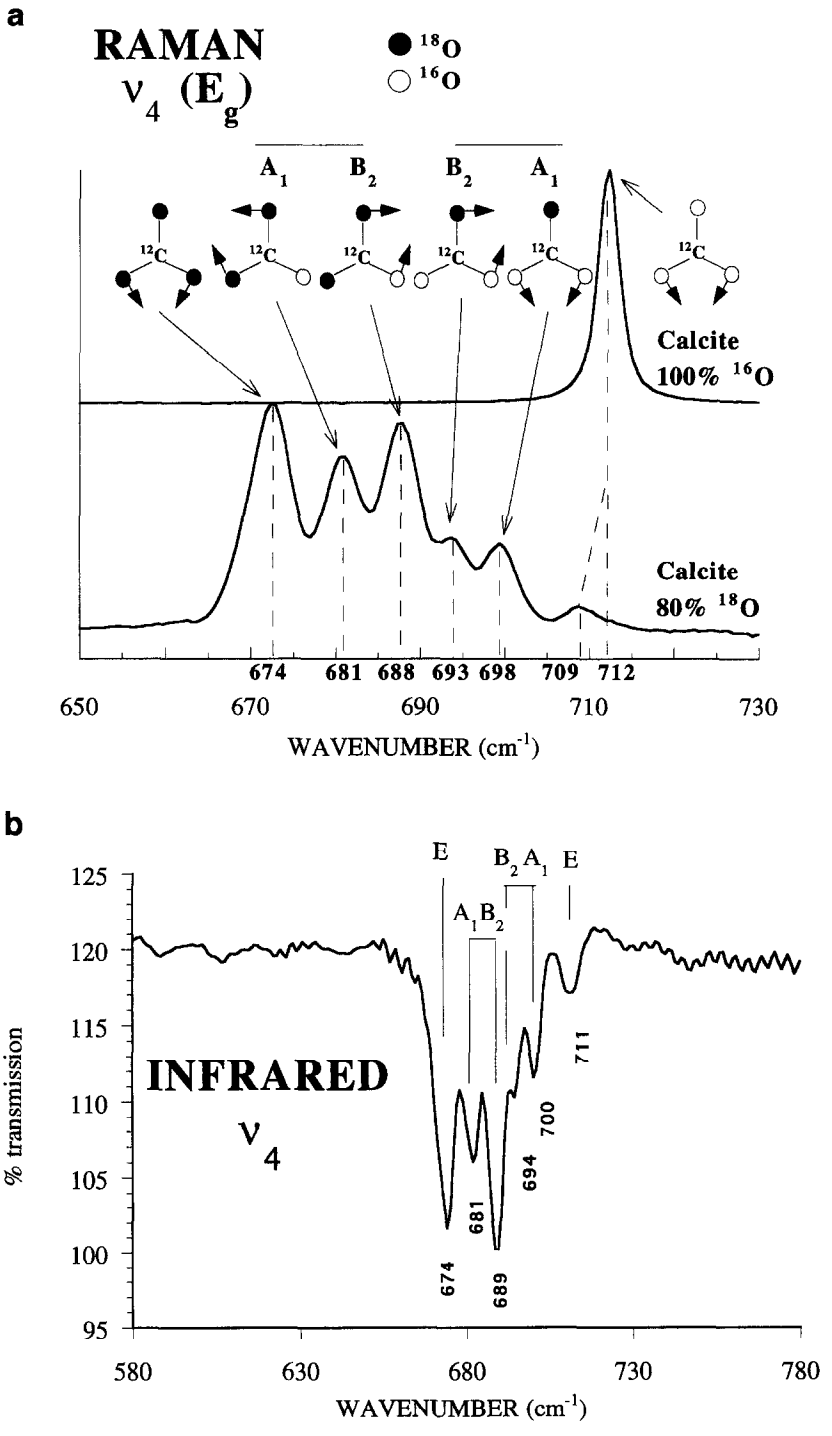

FIG. 3. (a) Raman spectra and associated motions of the ν_4 vibration of the CO_3^{2-} group in both $CaC^{16}O_3$ and partially substituted $CaC^{18}O_3$. (b) Infrared spectrum of the ν_4 vibration of the CO_3^{2-} group in partially substituted $CaC^{18}O_3$.

and $C^{16}O_2{}^{18}O$, respectively, and the unsubstituted component could give rise to the shoulder near 876 cm^{-1}.

A peak at 1800 cm^{-1} is easily observable in the IR spectrum of unsubstituted calcite samples (White, 1974), which must correspond to an overtone or combination band. Unlike the $2\nu_2$ combinations described in the previous paragraph, which appear near the same position in the Raman spectrum, this can not correspond to the first overtone of the ν_2 vibration, because both combinations ($A_{2g} \times A_{2g}$ and $A_{1g} \times A_{1g}$) have symmetry A_{1g} and are only Raman active. Based on a detailed analysis of the phonon spectrum of calcite and isostructural $NaNO_3$, Hellwege et al. (1970) suggested that

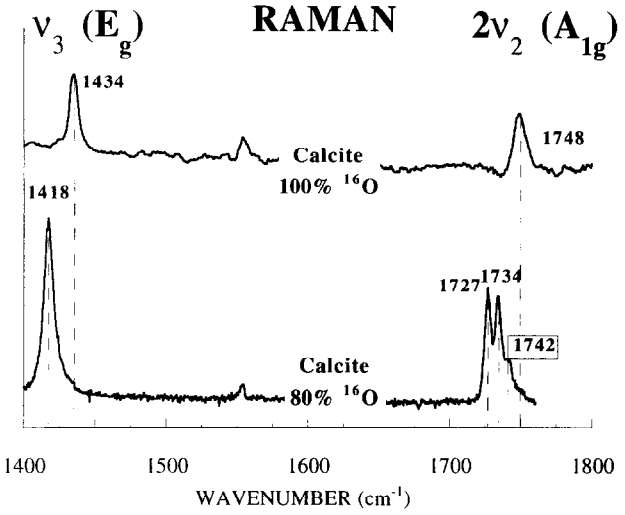

FIG. 4. Raman spectra of the ν_3 and $2\nu_2$ vibrations in pure ^{16}O calcite and in ^{18}O partially-substituted calcite.

the combination band near 1800 cm^{-1} was composed of contributions from combination of the ν_3 asymmetric stretch and the ν_6 and ν_8 external modes of the carbonate groups and Ca^{2+} ions (following the mode assignments suggested by White, 1974). The results of our isotopic substitution experiment suggest a completely different assignment. The isotopically substituted calcite shows a series of well-separated peaks at 1794, 1762, 1730, and 1697 cm^{-1} (Fig. 6). This is reminiscent of the peak splitting pattern already observed for the ν_1 and ν_4 internal modes of the carbonate groups in the partially isotopically substituted structure, described above. There is an excellent fit between the observed frequencies between 1800 cm^{-1} and 1700 cm^{-1}, and the $\nu_1 + \nu_4$ (IR) combinations of the isotopically substituted CO_3^{2-} groups (Table 1).

The close correspondence between the calculated and observed combination frequencies suggests that this is indeed a more appropriate assignment for the peak observed near 1800 cm^{-1} in the IR spectrum of pure calcite. The lack of any substantial peak broadening in the overtone bands suggests that the ν_1 and ν_4 internal modes are essentially dispersionless, which is reasonable for these internal vibrations of the carbonate groups. This is in contrast to the ν_3 vibration, proposed by Hellwege et al. (1970) to form one component of the combination band near 1800 cm^{-1}. This is an important observation for construction of the model frequency spectrum for calculation of the thermodynamic properties, discussed below, in which the fundamentals are treated as Einstein oscillators (see for instance Salje and Viswanathan (1976) and Kieffer (1979) for a similar treatment in the case of calcite). In addition, the close correspondence between the summed frequencies of the $\nu_1 + \nu_4$ fundamentals and the observed combination frequencies indicates that these vibrations are highly harmonic. This is also important for the thermodynamic calculation and is in agreement with our previous measurement of mode anharmonicities in calcite (Gillet et al., 1993; see also Appendix).

In the region of the low frequency external modes, two peaks appear in the Raman spectrum of the partly substituted sample at 268 and 147 cm^{-1} (Fig. 7). These correspond to the hindered translation and libration (about (0001) axes) of the carbonate groups (ν_{13} and ν_{14} in the notation of White, 1974). The precise assignment of these modes is not yet completely resolved, although it appears that the higher frequency mode has more translational character (Gillet et al., 1993). Both vibrations are highly anharmonic (Gillet et al., 1993). This most likely explains the lack of peak structure for the partially isotopically substituted sample, compared with the high frequency internal modes. The low frequency Raman modes have a form which is nearly Lorentzian, and a linewidth determined by anharmonic processes (Sakurai and Sato, 1971; Gillet et al., 1993). The higher frequency mode has an ^{18}O-induced isotope shift of -15 cm^{-1} (compared with an expected shift of -14 cm^{-1} ($\sqrt{\mu_{C^{16}O_3}/\mu_{C^{18}O_3}} = 0.9535$, for a fully substituted sample within the harmonic approximation) for the hindered translation of the CO_3^{2-} groups. In fact, because the isotopic substitution is only ~80%, the frequency for a fully substituted sample would lie at lower wavenumber, at approximately 265 cm^{-1}. The isotopic shift for the lower frequency librational mode is -9 cm^{-1}, consistent with the expected shift ($\sqrt{m_{16_O}/m_{18_O}} = 0.9428$) for that libration. The frequency for a fully substituted sample would lie near 146 cm^{-1}. The isotopic frequency shifts of these two modes, along with their intrinsic anharmonic behaviour, is extremely important in determining their isotopic fractionation characteristics, discussed below.

The detailed interpretation of the low frequency IR spectrum is less straightforward, because of the occurrence of overlapping modes, and the presence of TO-LO splitting (Hellwege et al., 1970; Onomichi and Kudo, 1971). The lowest frequency mode of unsubstituted calcite is of A_{2u} symmetry and lies at 92 cm^{-1} (TO). The corresponding LO component occurs at 132 cm^{-1}. This A_{2u} component is overlapped by an E_u mode at 102 cm^{-1} (TO) – 123 cm^{-1} (LO) (White, 1974; Hellwege et al., 1970). The powder transmission spectrum of an unsubstituted calcite sample in this region is shown in Fig. 8. The observed band in fact

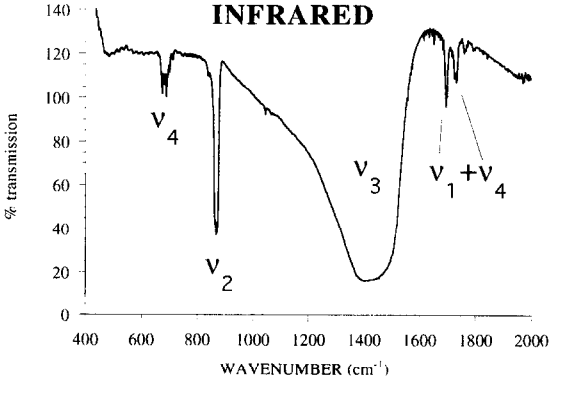

FIG. 5. Powder IR spectrum of isotopically substituted calcite showing the ν_2, ν_3, ν_4, and $\nu_1 + \nu_4$ vibrations.

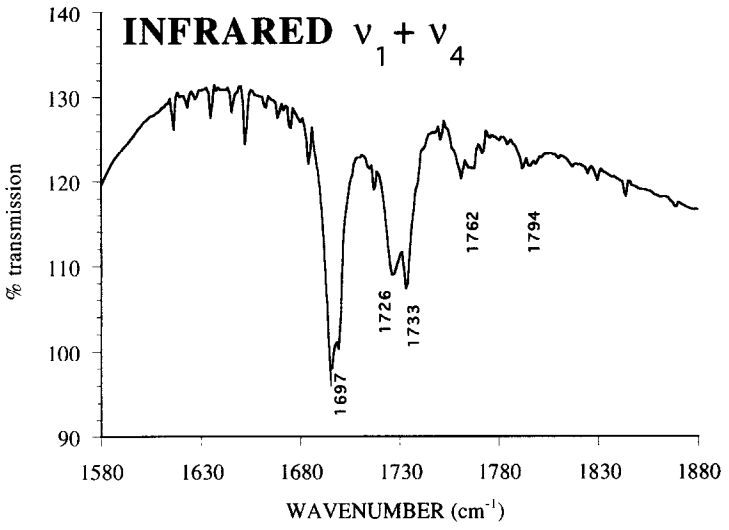

FIG. 6. Detailed IR spectrum of the $\nu_1 + \nu_4$ combination bands in partially substituted calcite.

closely resembles an unpolarized reflectance spectrum, with a low frequency edge near the TO mode frequency at 92 cm^{-1}, and a high frequency limit close to the zero in the reflectivity function at the LO mode (A_{2u}) frequency of 132 cm^{-1}. The E_u mode is unresolved within the band. The transmission minimum in the asymmetric peak occurs near 108 cm^{-1}, nearly coincident with the maximum in the reflectivity spectrum (Hellwege et al., 1970). The band profile of the isotopically substituted crystal is very similar, but with a slightly different asymmetry, and a small shift to lower frequency in the lower and upper edges of the transmission band (Fig. 8) (although the apparent band maximum hardly appears to shift). In the suggested mode assignment of White (1974), the A_{2u} vibrational mode (ν_7) corresponds to a libration of the CO_3^{2-} groups, which would be expected to give rise to an isotope shift of -5 cm^{-1}. This corresponds to the magnitude of the observed shift in the lower frequency edge of the transmittance band. The upper edge of the transmission band appears to show a larger frequency shift, perhaps indicating that the LO component is more affected by the isotopic substitution, but this is complicated by the presence of the unresolved E_u mode within the band.

The IR modes in the 100–400 cm^{-1} frequency range are shown in Fig. 9. The broad band in the 280–380 cm-1 region corresponds to the unresolved ν_6 (A_{2u}) and ν_8 (E_u) modes, which have a large TO-LO splitting. These are due to hindered translation and rotation of the carbonate groups (White, 1974), and our far-IR spectra show evidence for a large (~ -18 cm^{-1}) isotope shift, judging from the displacement of the low frequency edge of the maximum, which will lie closest to the TO frequency of the ν_6 band. The sharp peak with its maximum at 227 cm^{-1} corresponds to the ν_9 (E_u) vibration, which has a small TO-LO splitting (223–239 cm^{-1}) (Fig. 10). In this case, we find no clear evidence for an isotope shift in the band frequency. This is consistent with the assignment suggested by White (1974), who proposed that this vibration consisted of Ca^{2+} displacement only. There are also several weak, sharp peaks in this low frequency region, which we can not identify unambiguously (Fig. 9). A sharp peak occurs at 268 cm^{-1}. This corresponds exactly with the position of the Raman active translational mode (ν_{13}) for the partly substituted calcite (Fig. 7). It is possible that destruction of the inversion centre associated with the partial substitution has rendered some components of this mode infrared active, so that the ν_{13} vibration appears weakly in the IR spectrum. However, there is no correspond-

Table 1 : Combination table for $\nu_1 + \nu_4$ vibrations

ν_1		ν_4		$\nu_1+\nu_4$		
cm^{-1}	symmetry	cm^{-1}	symmetry	predicted	observed	symmetry
1023.5	A_1 (D_3)	674	E (D_3)	1697.5	1697	E (D_3)
1044.5	A_1 (C_{2v})	681	B_2 (C_{2v})	1725.5	1726	B_2 (C_{2v})
1044.5	A_1 (C_{2v})	689	A_1 (C_{2v})	1733.5	1733	A_1 (C_{2v})
1065.4	A_1 (C_{2v})	694	A_1 (C_{2v})	1759.4	1762 (unresolved)	A_1 (C_{2v})
1065.4	A_1 (C_{2v})	700	B_2 (C_{2v})	1765.4	1762 (unresolved)	B_2 (C_{2v})
1086.8	A_1 (D_3)	711	E (D_3)	1797.8	1794	E (D_3)

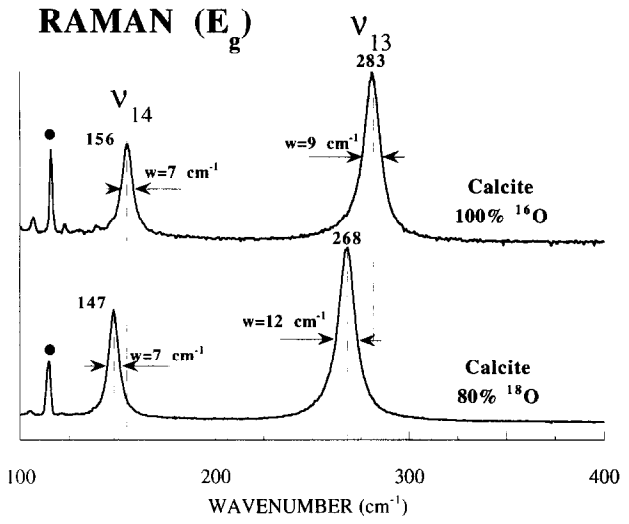

FIG. 7. Raman spectra of the E_g lattice modes of normal and ^{18}O-substituted calcite. ν_{13} and ν_{14} correspond to the nomenclature of White (1974). w indicates the bandwidth. The dots indicate plasma lines of the excitation laser.

ing peak at the position of the Raman active librational mode (ν_{14}, at 148 cm^{-1}), which is puzzling. The adjacent weak peak at 258 cm^{-1} could possibly correspond to the previously silent ν_{11} translational (A_{2g}) mode of the partly substituted calcite, which is expected in this region from neutron scattering measurements and lattice dynamical calculations (Cowley and Pant, 1973; Plihal, 1973). However, from experiments on dolomite ($CaMg(CO_3)_2$), we have previously assigned this silent mode to a position near 335 cm^{-1} in unsubstituted calcite (Gillet et al., 1993), which would bring it to near 319 cm^{-1} for $CaC^{18}O_3$, and no corresponding feature near 258 cm^{-1} is observed in the Raman spectrum. Finally, although it is at the limit of our noise resolution, a very weak feature appears reproducibly in our spectra near 162 cm^{-1}, which is absent from the unsubstituted calcite (Fig. 9). This could well correspond to the other low frequency silent A_{2g} librational mode (ν_{12}), which occurs near 172 cm^{-1} in normal calcite (Gillet et al., 1993), shifted and rendered weakly IR active by the partial substitution.

4. CONSTRUCTION OF A MODEL DENSITY OF STATES, AND CALCULATION OF THERMODYNAMIC PROPERTIES

4.1. Density of States Model

Detailed inelastic neutron scattering measurements have been made of the dispersion of low frequency phonon branches in calcite (Cowley and Pant, 1973; Plihal, 1973; Dove et al., 1992). These have permitted establishment of an experimental density of states function, by applying a polarizable ion model to fit the neutron data (Fig. 11a). It was initially our intent to simply take this $g(\omega)$ function and apply the anharmonic corrections and isotope shifts which we had determined experimentally to calculate the thermodynamic properties. However, it proved difficult to do this analytically, conserving the correct area ratios under portions of the $g(\omega)$ curve. For this reason, we chose to construct a simplified model density of states using the formalism developed by Kieffer (1979), in which groups of particular modes occupied optic continua or appeared as Einstein oscillators, with positions and bounds constrained by the infrared, Raman, and neutron data. Construction of this model for both $CaC^{16}O_3$ and $CaC^{18}O_3$ is described below.

We had no experimental data on the isotopic shift of the acoustic branches. The sound wave velocities in normal calcite are well known from the measurements of Robie and Edwards (1966). These define the initial slope of the acoustic branches. Kieffer (1979) has suggested a scheme for averaging these to construct the low frequency density of states due to acoustic branches. However, these models assume particular forms for the dispersion of the acoustic branches. If the models of Kieffer (1979) are applied to the case of calcite, this results in peaks in the low frequency model density of states which do not fit well with the observed form of the $g(\omega)$ function. This is because the acoustic modes at large q interact with the optic branches, resulting in maxima in $g(\omega)$ at lower wavenumber than expected. For this reason, we have chosen to slightly modify the averaged longitudinal and shear acoustic velocities (Table 2), to result in a $g(\omega)$ which better matches the experiment (Fig. 11b). Most of the area under $g(\omega)$ near 100 cm^{-1} results from the short wavelength acoustic branches which are mixed with librations of the CO_3^{2-} groups and Ca^{2+} translational modes (White, 1974), and so we have assumed similar anharmonic parameters (a_i) (see Appendix for definition) for these acoustic modes. This assumption is supported by the example of other highly anharmonic minerals like quartz (Gillet et al., 1990; Castex and Madon, 1995). To estimate the isotopic frequency shifts of these branches, we have followed the prescription of Kieffer (1979) for the longitunal and

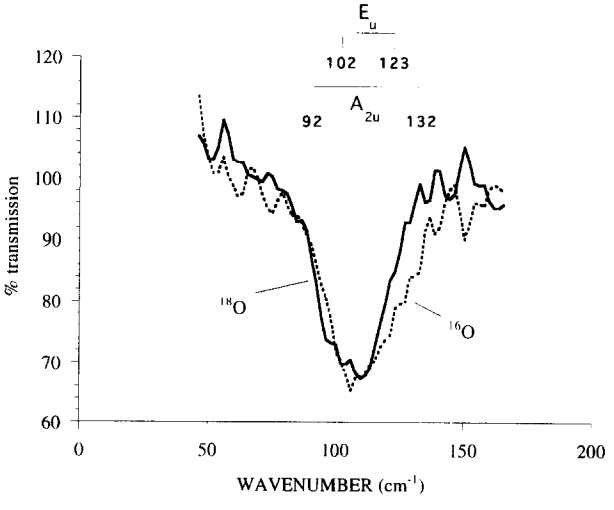

FIG. 8. Transmission IR spectra of the lattice modes of E_u and A_{2u} symmetry in both normal and ^{18}O-substituted calcite. The positions of the LO and TO branches are shown.

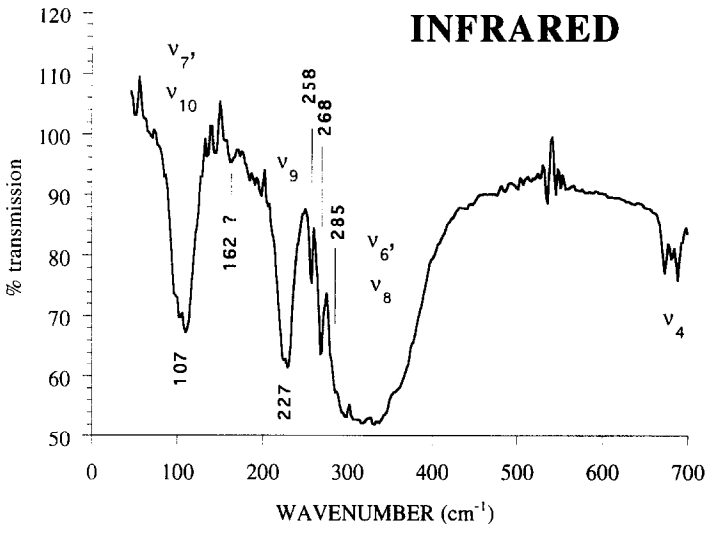

FIG. 9. Transmission IR spectrum of ^{18}O-substituted calcite showing the modes in the 100–400 cm^{-1} frequency range. The ν_i symbols refer to the notation of White (1974).

transverse modes. For the averaged LA branch, we have taken the square root of the molecular mass of the $CaCO_3$ unit (Table 2). For the shear (TA) branch, which resembles the lowest frequency optic mode with which it is mixed at large q, we have applied a −5% oxygen isotope shift, consistent with the measured value for the A_{2u} and E_u modes (observed shift −5 cm^{-1}, near 100 cm^{-1}), discussed below.

The next set of modes concerns the low frequency optic branches. There are two infrared active modes (A_{2u} and E_u symmetries) which have similar anharmonic parameters (a_i = -15.10^{-5} K^{-1}, Gillet et al., 1993) and isotopic shifts (−5 cm^{-1}). The lower bound for normal calcite is fixed at 92 cm^{-1} by the zone centre TO frequency, and this band extends to 150 cm^{-1}, close to the IR active LO mode frequency (White, 1974). For the low frequency Raman mode at 156 cm^{-1}, due to CO_3^{2-} libration, we have introduced a narrow continuum between 150 and 170 cm^{-1}, to account for effects of dispersion (Cowley and Pant, 1973; Plihal, 1973; Dove et al., 1992) (Fig. 11). This mode also has a large anharmonic parameter (a_i = -15.10^{-5} K^{-1}), and a measured isotope shift of −8 cm^{-1} which is extended to −10 cm^{-1} for a fully substituted calcite.

The next continuum extends from 132–300 cm^{-1}, and contains the IR active modes A_{2u} + E_u and one inactive A_{2g} mode. The limits for this continuum are fixed by the infrared and neutron data, and dispersion of the branches in this region is fairly homogeneous (Cowley and Pant, 1973; Plihal, 1973). These modes are quite harmonic (a_i = -1.10^{-5} K^{-1}), and our data suggest that these modes are not affected by the isotopic substitution.

The final continua in the low frequency density of states concern the IR modes (E_u and A_{2u}) between 300 and 400 cm^{-1}, and the inactive A_{2g} mode estimated to occur near 300–310 cm^{-1} (Cowley and Pant, 1973; Plihal, 1973; Gillet et al., 1993). The anharmonicity of the E_u and A_{2u} modes is also taken to be small (a_i = -1.10^{-5} K^{-1}), and they have

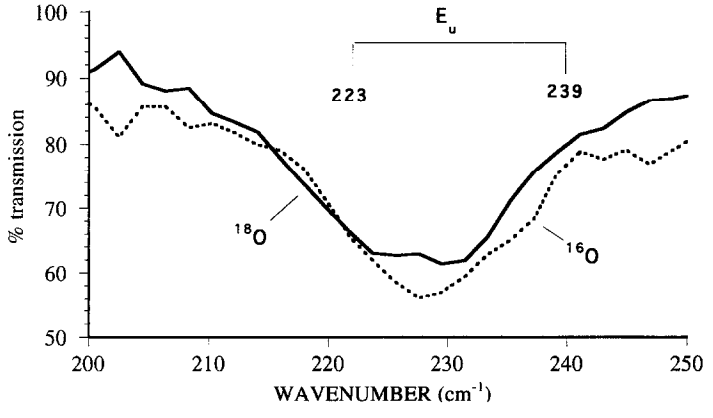

FIG. 10. Detailed view of the IR-active E_u mode near 230 cm^{-1} in both normal and ^{18}O-substituted calcite.

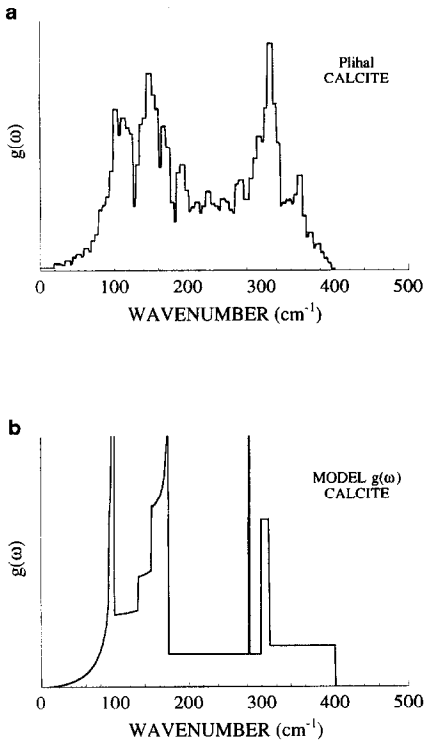

FIG. 11. (a) Density of states for the lattice modes of calcite calculated by Plihal (1973) from neutron scattering data. (b) Simplified density of states for the lattice modes of calcite used in this study.

a strong isotope shift of -15 cm ^{1}. This shift is assumed constant across the entire band. Because we have no experimental information on the isotope shift of the A_{2g} mode, we have left it at the same position for substituted calcite, i.e., between 300 and 310 cm^{-1}. We have placed the nearly dispersionless Raman active mode (E_g) as an Einstein oscillator at 283 cm^{-1}. This has a large anharmonicity ($a_i = -15.10^{-5}\ K^{-1}$) and isotope shift ($-18\ cm^{-1}$).

In the high frequency region, the internal modes ν_1, ν_2, and ν_4 give rise to branches which are nearly dispersionless (Plihal, 1973), which can be modelled by sharp peaks in the $g(\omega)$ function (Fig. 12). To account for the effect of the isotopic substitution, we have moved these peaks by appropriate amounts taken from our Raman and infrared study, to construct the model density of states for $CaC^{18}O_3$ (Table 2). The ν_3 vibration shows a larger dispersion, presumably because of the large TO-LO splitting associated with long range electrostatic interactions accompanying the asymmetric stretching vibration (Plihal, 1973). This gives rise to a broad asymmetric band in $g(\omega)$, extending from near 1400 to 1550 cm^{-1} (Plihal, 1973; Salje and Viswanathan, 1976; Fig 12). To model the effect of ^{18}O substitution, we have shifted this entire band by $-23\ cm^{-1}$ to lower frequency (Table 2), which corresponds to the observed shift of the peak maximum in our powder IR study (Fig. 5).

At this point, we have constructed model density of states functions $g(\omega)$ for $CaC^{16}O_3$ and $CaC^{18}O_3$ (Table 2). They are then used to calculate the thermodynamic functions as a function of temperature and pressure within the harmonic and anharmonic approximations, using the methods of statis-

Table 2 : Data used for the construction of the density of states of the vibrational modes of calcite. The parameters q and m are defined in the appendix. The numbers in italics refers to the density of states for $CaC^{18}O_3$.

TYPE	freqency (cm^{-1}) / speeds ($m.s^{-1}$)	number of oscillators	Grüneisen parameter	Anharmonic parameter ($10^5\ K^{-1}$)	q	m
Acoustic	6500 - *6313*	1	+0.45	-15	1	0
Acoustic	3700 - *3500*	1	-2.25	-15	1	0
Acoustic	3700 - *3500*	1	-2.25	-15	1	0
optic continuum	92 ---> 150 *87 ---> 150*	3	1.3	-0.23	1	0
optic continuum	132 ---> 300 *132 ---> 300*	4	1.3	-1	1	0
optic continuum	150 - 170 *140 - 160*	2	1.3	-15	1	0
optic continuum	300 ---> 310 *300 ---> 310*	1	1.3	-1	1	0
optic continuum	300 ---> 400 *285 ---> 385*	3	1.3	-1	1	0
optic continuum	1407 ---> 1549 *1384 ---> 1526*	4	0.46	-1.3	1	0
Einstein oscill.	283 - *265*	2	1.4	-15	1	0
Einstein oscill.	711 - *673*	4	0.23	-0.23	1	0
Einstein oscill.	880 - *864*	2	-0.04	-0.34	1	0
Einstein oscill.	1085- *1024*	2	0.40	-0.10	1	0

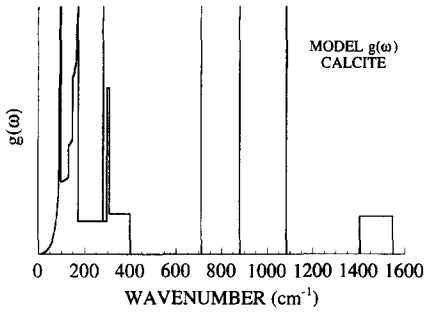

FIG. 12. Complete vibrational density of states of calcite including lattice modes and internal modes of the CO_3^{2-} groups.

tical thermodynamics. The formulae used for these calculations are outlined in the Appendix.

4.2. Heat Capacity and Entropy

The actual heat capacity at constant volume C_V (Fig. 13) can be obtained from C_P measurements (Kobayashi 1951; Staveley and Linford 1969; Jacobs et al., 1981) and the high-temperature measurements of the coefficient of thermal expansion α by Markgraf and Reeder (1985) and existing data on the bulk modulus K_0 = 72 GPa (Fiquet et al., 1994) using the relation

$$C_P = C_V + \alpha(T)^2 V(T) K_0(T) T.$$

C_V can also be calculated from the two density of states functions shown in Figs. 11 and 12 using the formula developed in the Appendix. Within the harmonic approximation, i.e., setting $a_i = 0$, both $g(\omega)$ models lead to values in agreement to each other to within 1% from 0–1200 K and similar to those proposed by Plihal (1973). However, the harmonic calculations strongly underestimate the actual values of C_V above 300 K and do not account for values exceeding the Dulong-Petit (3nR) limit above 800 K (Fig. 13 and Table 3). A difference of the order of 10% is observed at 1200 K (Table 3). Nevertheless, these calculations confirm that the simplified density of states model of Fig. 11b is representative of the more detailed density of states of Fig. 11a.

Similar calculations were carried out including anharmonic corrections provided by the spectroscopically measured a_i parameters (Gillet et al., 1993: see Appendix). In that case, the calculated values of C_V agree to within 1% of the actual C_V inferred from calorimetric and volumetric measurements (Fig. 13) between 50 and 1200 K. This level of agreement lends confidence to our anharmonic modelling of the thermodynamic properties of calcite. As will be shown in the next section, values for the volume (V), thermal expansion (α), and bulk modulus (K) can also be calculated, permitting an estimate of the $\alpha^2 VKT$ term, and thus direct calculations of C_P (Fig. 14 and Table 3).

The entropy can also be calculated from expression (9) given in the Appendix. Excellent agreement is only observed with experiment, if anharmonicity is taken into account (Fig. 15 and Table 3).

4.3. Equation of State

From the thermal (vibrational) Helmoltz free energy it is possible to derive an expression for the equation of state (EOS) at high-pressure and temperature (Guyot et al., 1996; see Appendix relations 12, 13, and 14). We use a Mie-Grüneisen EOS:

$$P = P_{300\,K} + (P_{th} - P_{th\,300\,K}),$$

where $P_{300\,K}$ is the static pressure at 300 K, obtained by fitting available experimental room temperature compression data to a third order Birch Murnaghan EOS (Fiquet et al., 1994):

$$P_{300\,K} = \frac{3}{2} K_0 \left[\left(\frac{V_0}{V}\right)^{7/3} - \left(\frac{V_0}{V}\right)^{5/3} \right] \times \left[1 + \frac{3}{4}(K_0' - 4) \left(\left(\frac{V_0}{V}\right)^{2/3} - 1 \right) \right].$$

P_{th} and $P_{th\,300\,K}$ represent the thermal pressure at a given pressure and temperature and the thermal pressure at 300 K, respectively. For calcite we took K_0 = 72 GPa and K_0' = 5.37 (Fiquet et al., 1994). P_{th} is calculated by:

$$P_{th} = -\left(\frac{\partial F_{vib}}{\partial V}\right)_T.$$

Two mode anharmonic parameters, a_i and m_i, are involved in the expression of the thermal pressure (see Appendix). Because we have neither experimental measurements nor theoretical estimates of the m_i parameters, they are set equal to 0. Under these conditions, only a quasi-harmonic calculation of the EOS can be performed, in contrast to C_V and S.

Figure 16a and Table 4 present a comparison between calculated and experimental volumes at high temperature and room pressure. They agree to within 1%. The coefficient of thermal expansion can also be calculated at various pressures (Fig. 16b). α decreases linearly with pressure between 10^5 Pa and 3 GPa, with $(\partial\alpha/\partial P)_T = -1.46\ 10^{-6}\ K^{-1}$/GPa, $-1.94\ 10^{-6}\ K^{-1}$/GPa, $-2.43\ 10^{-6}\ K^{-1}$/GPa at 300, 700,

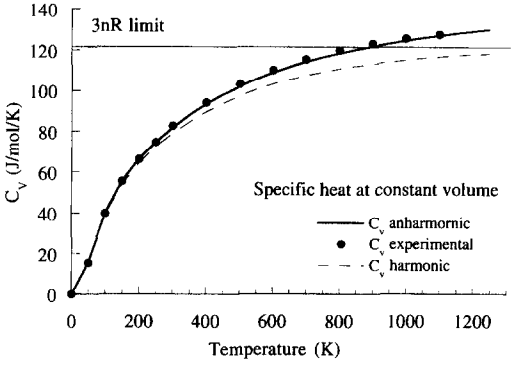

FIG. 13. Specific heat at constant volume (C_V) of calcite calculated with harmonic assumptions and with anharmonic corrections. Comparison with C_V derived from calorimetric measurements of C_P, thermal expansion, and bulk modulus using the relation $C_P = C_V + \alpha^2 VKT$.

Table 3 : Specific heat and entropy of calcite. C_{Pexp} and S_{exp} are experimental measurements from Staveley and Linford (1969) and Jacobs et al. (1981). C_{Vh} (specific heat at constant volume) and S_h (entropy) are values calculated with the vibrational model and with harmonic assumptions. C_{Va} and S_a are similar quantities calculated with anharmonic corrections. C_{Ph} and C_{Pa} represent the specific heat at constant pressure obtained by adding to C_{Vh} or C_{Va} the calculated correction term α^2VKT obtained from the EOS calculated with the vibrational model. $C_V + cor$ is obtained by adding C_{Vh} to the α^2VKT term calculated in that case from available high temperature measurements of the molar volume of calcite by Markgraff and Reeder (1985).

	J/mol/K								
T(K)	Cvh	Sh	Cva	Sa	Cpexp	Sexp	Cv+cor	Cph	Cpa
0	0.00	0.00	0.00	0.00	0.00	0.00	0.00	0.0000	0.0000
50	15.01	6.01	15.48	6.48	15.19	6.79	15.48	15.010	15.480
100	38.80	24.23	39.74	25.16	39.19	25.14	39.74	38.820	39.760
150	53.97	43.08	55.37	44.49	55.38	44.33	55.37	54.070	55.470
200	64.26	60.14	66.12	62.00	66.50	61.86	66.12	64.450	66.320
250	72.25	75.42	74.58	77.75	75.65	77.70	74.62	72.560	74.900
300	78.91	89.27	81.71	92.07	83.74	92.22	81.79	79.350	82.150
350	84.61	101.95	87.88	105.21	89.90	105.60	88.02	85.180	88.450
400	89.52	113.66	93.26	117.39	94.90	118.00	93.47	90.230	93.960
450	93.76	124.54	97.96	128.74	99.20	129.40	98.27	94.610	98.810
500	97.41	134.71	102.08	139.38	103.30	140.10	102.50	98.410	103.10
550	100.55	144.25	105.68	149.38	107.10	150.10	106.25	101.70	106.80
600	103.25	153.22	108.85	158.82	110.70	159.60	109.59	104.60	110.20
650	105.57	161.69	111.64	167.76	114.10	168.60	112.57	107.00	113.10
700	107.58	169.71	114.11	176.24	117.20	177.10	115.27	109.20	115.80
750	109.31	177.31	116.32	184.31	119.90	185.30	117.73	111.10	118.10
800	110.82	184.53	118.29	192.00			119.98	112.80	120.30
850	112.13	191.42	120.07	199.35			122.08	114.30	122.20
900	113.28	197.99	121.68	206.39			124.03	115.60	124.00
950	114.29	204.27	123.15	213.14			125.87	116.80	125.70
1000	115.17	210.29	124.51	219.63			127.63	117.90	127.20
1050	115.96	216.07	125.76	225.87			129.08	118.80	128.60
1100	116.65	221.62	126.92	231.89			130.57	119.70	130.00
1150	117.27	226.97	128.01	237.70			131.96	120.60	131.30
1200	117.83	232.12	129.03	243.32			133.28	121.30	132.50
1250	118.33	237.09	129.99	248.75			134.54	122.00	133.70

and 1200 K, respectively. The isothermal bulk modulus decreases linearly with temperature $(\partial K/\partial T)_P = -0.011$ GPa/K with no dependence upon pressure between 10^5 Pa and 3 GPa. Finally, $K' = (\partial K/\partial P)_T$ decreases from 5.37–4.72 between 300 and 1200 K.

4.4. Isotopic Fractionation

The reduced partition function ratio of calcite is equal to the equilibrium constant for exchange of one isotopic atom between calcite and oxygen gas:

$$\tfrac{1}{3}CaC^{16}O_3 + \tfrac{1}{2}{}^{18}O_2 \leftrightarrow \tfrac{1}{3}CaC^{18}O_3 + \tfrac{1}{2}{}^{16}O_2.$$

The reduced partition function ratio of calcite f can be calculated from the Helmoltz free energy of both $CaC^{16}O_3$ (F) and $CaC^{18}O_3$ (F^*) according to the following relation:

$$\ln f = \frac{F - F^*}{3RT} + \frac{3}{2}\ln\left(\frac{m}{m^*}\right),$$

where m and m^* are the respective masses of O^{16} and O^{18} (Kieffer, 1982).

There have been several attempts to calculate f from mi-

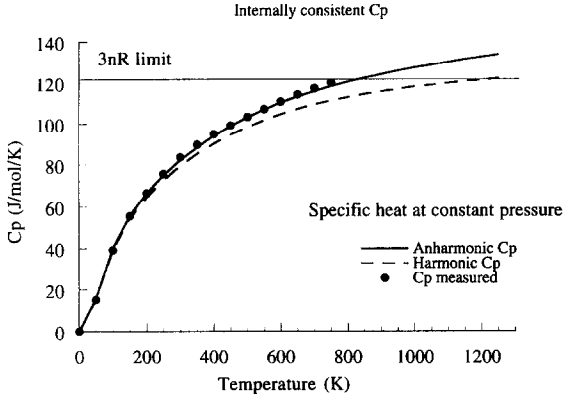

FIG. 14. Comparison between measured and calculated C_P. Experimental data from Staveley and Lindford (1969) and Jacobs et al. (1981).

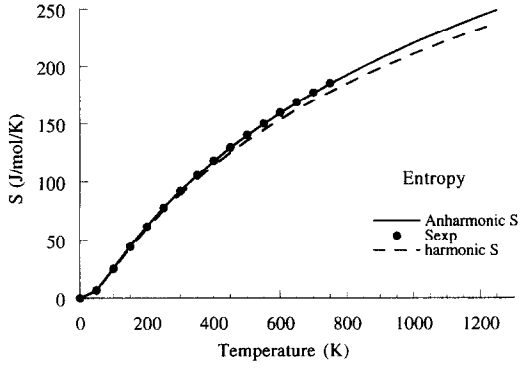

FIG. 15. Entropy (S) of calcite calculated with harmonic assumptions and with anharmonic corrections. Comparison with S derived from calorimetric measurements.

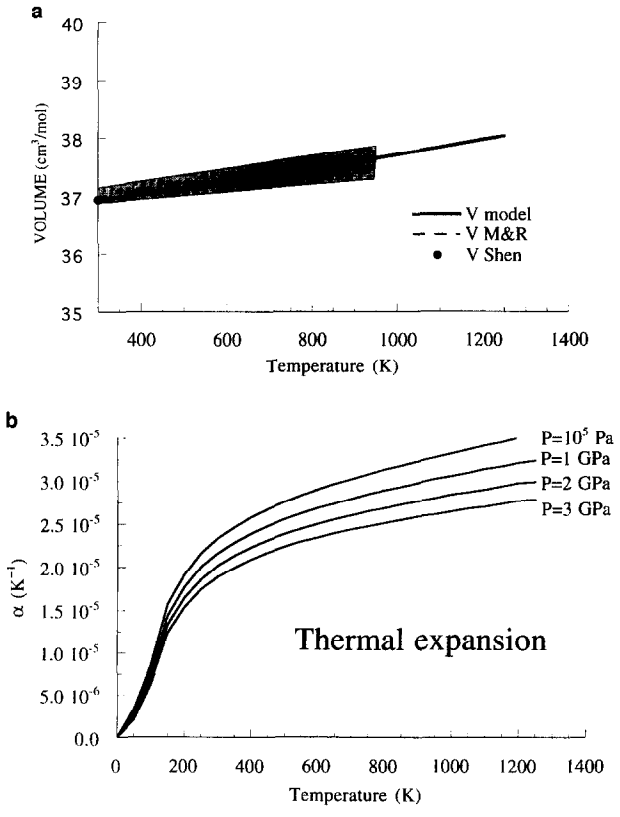

FIG. 16. (a) Calculated molar volume of calcite at room pressure as a function of temperature compared with the experimental measurements of Markgraf and Reeder (1985) and Chen et al. (unpubl. results). The shaded area represents the field of all available measurements. (b) Pressure and temperature dependence of the coefficient of thermal expansion.

croscopic models. Bottinga (1968) used a set of published force constants to calculate the frequencies of the 30 vibrations of both $CaC^{16}O_3$ and $CaC^{18}O_3$ calcite, from which he derived f. Kieffer (1982) used her simplified density of states model, and took the calculated shifts of Bottinga for twelve of the eighteen lattice modes and determined the shifts of the remaining six lattice modes by a high temperature product rule which ensures that the reduced partition function goes to one at high temperature. It must, however, be noticed that this rule is not necessary in a valid formulation of the statistical thermodynamics treatment of isotopic exchange. Following O'Neil et al. (1969), Chacko et al. (1991) have separated internal from lattice vibrations and calculated a single heat capacity term for the latter. They then determined the appropriate isotopic shift by application of the high temperature product rule. Dove et al. (1992) have calculated f from an interatomic potential model for calcite.

Our purpose is to use the experimentally obtained Raman and IR spectroscopic data to demonstrate the effects of anharmonicity and high pressure on the calculated values of f. We do not attempt to reproduce expected values of the reduced partition function ratio of calcite derived from exchange experiments between CO_2 or H_2O and calcite. This could be done, as discussed by Clayton and Kieffer (1991) and Chacko et al. (1991), by combining laboratory experiments and statistical thermodynamical calculations. Moreover, the effect of pressure or anharmonicity on the reduced partition function ratio of calcite cannot be inferred directly from experiments at high pressures involving exchange between calcite and other minerals or fluids. In fact, pressure can affect in a different way the reduced partition function ratio of the exchanging fluids or minerals and the effect on the overall isotopic exchange can be hindered by canceling effects.

We have calculated F^* and F taking into account our measured Raman and infrared isotopic shifts for ^{18}O-substituted calcite. As discussed above, we do not have isotopic shift data for all modes. This is the case for the inactive ν_{11} and ν_{12} A_{2g} modes estimated to occur near 300–310 cm^{-1} and 170–200 cm^{-1}, respectively, and for the mode ν_5 of A_{2u} symmetry. We have assumed that these modes are not affected by the isotopic substitution, by comparison with the behaviour of modes involving similar atomic motions and for which the isotopic shifts have been measured in the present work. The ν_5 mode involves only motions of the Ca^{++} ions (White, 1974) and is thus expected to be insensitive to the ^{18}O substitution like the ν_9 mode for which no isotopic shift has been evidenced in the present measurements. The ν_{11} and ν_{12} modes involve motions similar to that of the ν_{10} mode which has only a small isotopic shift. We have not used the high-temperature product rule proposed by Kieffer (1982) in any of our calculations. The results are presented in Table 5 along with the data from other studies.

Table 4 : Comparison between calculated and measured volumes (Markgraf and Reeder, 1985) of calcite at high temperature and room pressure.

T(K)	V_{model}	V_{exp}
	cm3/mol	
300	36.94	36.94
350	36.98	36.98
400	37.03	37.03
450	37.08	37.08
500	37.13	37.14
550	37.18	37.20
600	37.24	37.27
650	37.29	37.33
700	37.35	37.41
750	37.40	37.48
800	37.46	37.56
850	37.52	37.65
900	37.58	37.74
950	37.64	37.83
1000	37.70	
1050	37.77	
1100	37.83	
1150	37.90	
1200	37.96	
1250	38.03	

Table 5 : Reduced partition function ratio of calcite (1000 lnf) calculated at various pressure and temperature conditions under quasi-harmonic or anharmonic assumptions. Comparisons with calculated values from Kieffer (1982), Chako et al. (1991) and Dove et al. (1992).

		1000 lnf				
T (K)	P (GPa)	quasi harmonic	anharmonic	Kieffer	Dove	Chacko
300	0	98.96	97.57	98.5	94.3	98.03
	1	98.98	97.59			
	2	98.99	97.59			
	3	99.03	97.63			
500	0	41.53	39.20	41.43	39.35	41.43
	1	40.97	38.63			
	2	40.45	38.14			
	3	40.01	37.68			
700	0	23.09	19.83			22.43
	1	22.24	18.98			
	2	21.50	18.25			
	3	20.82	17.56			
1000	0	13.56	8.92	11.38	10.82	11.40
	1	12.44	7.78			
	2	11.44	6.78			
	3	10.55	5.90			
1200	0	11.39	5.81			8.00
	1	10.08	4.50			
	2	8.95	3.36			
	3	7.93	2.35			

Both quasi-harmonic and anharmonic calculations of 1000 ln (f) are in good agreement with those recommended by Clayton and Kieffer (1991) and Chacko et al. (1991) in the 300–1200 K temperature range. Up to 700 K the discrepancy is within ±2%. At higher temperatures the values of Chacko et al. (1991) lie between those obtained by the quasi-harmonic and anharmonic calculations (Table 5).

The slight difference probably originates from the unknown shifts of the silent modes, for which we assumed no isotopic shift or because we have taken fundamental frequencies rather than zero-order-frequencies and neglected the ground state anharmonicity of the vibrations. Nevertheless, our calculations can be used to demonstrate the effects of anharmonicity and of high pressures on the isotope shift. Anharmonic corrections lead to lower values of 1000 ln (f) when compared to harmonic calculations (Table 5). The difference is significant, 3% at 300 K and 30% at 1000 K, pointing out the need to include anharmonicity in calculations of the reduced partition function for highly anharmonic minerals like calcite or quartz.

1000 ln (f) has also been caclulated at high pressures (Table 5). The effect of high pressures is very small at 300 K but becomes significant at higher temperatures. At 1000 K, 1000 ln (f) decreases from 13.56 at 10^5 Pa to 10.55 at 3 GPa. Polyakov and Kharlashina (1994) have used the Kieffer (1979) model to calculate the effect of pressure on f within a quasi-harmonic treatment. They found that pressure modifies f significantly, but the effect is more pronounced at low temperature than at high temperature, which is in contradiction with the present calculations. For instance, they report the following values of $\Delta = 1000\ (\ln f_{(1\text{GPa})} - \ln f_{(10^5\text{Pa})})$ for calcite: +0.7 at 300 K and +0.1 at 1000 K, while we found +0.02 at 300 K and −1.11 at 1000 K. The origin of this discrepancy between the two calculations is probably linked to the difference in assumptions. The present calculations show that pressure has a significant effect on the reduced partition function ratio of calcite and that anharmonicity which is strong in calcite must be taken into account. However, further theoretical insights are badly needed to assess the present calculated effect of pressure.

5. CONCLUSIONS

From the infrared and Raman vibrational spectra of ($CaC^{16}O_3$) and ($CaC^{18}O_3$) calcite we have constructed a simplified density of states of the vibrational modes. This density of states has been used to calculate the thermodynamic properties of calcite using anharmonic corrections obtained from previously measured pressure and temperature-induced shifts of the Raman modes. The results show that anharmonic calculations, unlike harmonic ones, are in excellent agreement with existing measurements of heat capacity and molar volume at low (50 K) and high temperature (1200 K). The dependence upon pressure of the coefficient of thermal expansion can be estimated at various pressure and temperature conditions from the calculated EOS. Finally the reduced partition function ratio of calcite has been calculated at room pressure and at high temperature. The results show that anharmonicity cannot be neglected in the calculations of 1000 ln (f) and that pressure has a nonnegligible effect.

Acknowledgments—This work has been supported by the INSU/CNRS department and the program DBT Terre Profonde. PFM and AG were supported by NSF grant EAR-9219504. We wish to warmly thank F. Guyot for checking all the mathematical expressions used throughout this paper and for exciting discussions. S. F. Sheppard was our consultant for the geochemical aspect of isotopic fractionation. The constructive reviews of Dr. Bottinga and Dr. O'Neil were greatly appreciated.

Editorial handling: F. J. Ryerson

REFERENCES

Bottinga Y. (1968) Calculation of fractionation factors for carbon and oxygen isotopic exchange in the system calcite-carbon dioxide-water. *J. Phys. Chem.* **72**, 800–807.

Chacko T., Mayeda T. K., Clayton R. N., and Goldsmith J. R. (1991) Oxygen and carbon isotope fractionation between CO_2 and calcite. *Geochim. Cosmochim. Acta* **55**, 2867–2882.

Castex J. and Madon M. (1995) Test of the vibrational modelling for the lambda-type transitions: Application to the alpha-beta quartz transition. *Phys. Chem. Miner.* **22,** 1–10.

Catti M., Pavese A., and Price G. D. (1993) Thermodynamic properties of $CaCO_3$ calcite and aragonite: a quasi-harmonic calculation. *Phys. Chem. Mineral.* **19,** 472–479.

Clayton R. N. and Kieffer S. W. (1991) Oxygen isotopic thermometer calibrations. In *Stable Isotope Geochemistry: A Tribute to Samuel Epstein* (ed. H. P. Taylor Jr. et al.), pp. 316. McMillan.

Cloots R. (1991) Raman spectrum of carbonates $M^{II}CO_3$ in the 1100–1000 cm^{-1} region: observation of the v1 mode of the isotopic $(C^{16}O_2{}^{18}O)^{2-}$ ion. *Spectrochim. Acta* **47A,** 1745–1750.

Cowley E. R. and Pant A. K. (1973) Lattice dynamics of calcite. *Phys. Rev. B* **8,** 4795–4800.

Dove M. T., Winkler B., Leslie M., Harris M. J., and Salje E. K. H. (1992) A new interatomic potential model for calcite: applications to lattice dynamics studies, phase transition, and isotope fractionation. *Amer. Mineral.* **77,** 244–250.

Fiquet G., Gillet P., and Richet P. (1992) Anharmonic contributions to the heat capacity of minerals at high-temperatures. Application to Mg_2GeO_4, Ca_2GeO_4, $MgCaGeO_4$. *Phys. Chem. Mineral.* **18,** 469–479.

Fiquet G., Guyot F., and Itie J. P. (1994) High-Pressure X-Ray Diffraction Study of Carbonates-$MgCO_3$, $CaMg(CO_3)_2$, and $CaCO_3$. *Amer. Mineral.* **79,** 15–23.

Gillet P., Guyot F., and Malezieux J. M. (1989) High-pressure and high-temperature Raman spectroscopy of Ca_2GeO_4: some insights on anharmonicity. *Phys. Earth Planet. Intl.* **58,** 141–154.

Gillet P., Le Cléach A., and Madon M. (1990) High-temperature Raman spectroscopy of the SiO_2 and GeO_2 polymorphs: anharmonicity and thermodynamic properties at high-temperature. *J. Geophys. Res.* **95,** 21635–21655.

Gillet P., Richet P., Guyot F., and Fiquet G. (1991) High-temperature thermodynamic properties of forsterite. *J. Geophys. Res.* **96,** 11805–11816.

Gillet P., Fiquet G., Malézieux J. M., and Geiger C. (1992) High-pressure and high-temperature Raman spectroscopy of end-member garnets: pyrope, grossular and andradite. *Eur. J. Mineral.* **4,** 651–664.

Gillet P., Biellmann C., Reynard B., and McMillan P. F. (1993) Raman spectroscopic studies of carbonates. Part I: High-pressure and high-temperature behaviour of calcite, magnesite, dolomite, aragonite. *Phys. Chem. Mineral.* **20,** 1–18.

Guyot F., Wang Y., Gillet P., and Ricard Y. (1996) Experimental measurements of high-pressure high-temperature volumes in olivines by synchrotron X-Ray diffraction. Comparison with quasi-harmonic computations. *Phys. Earth Planet. Intl.*

Hellwege K. H., Lesch W., Plihal M., and Schaack G. (1970) Zwei-Phononen-Absorptionsspektren und Dispersion der Schwingungszweige in Kristallen der Kalkspatstruktur. *Z. Phys.* **232,** 61–86.

Herzberg G. (1945) *Molecular spectra and molecular structure. II. Infrared and Raman spectra of polyatomic molecules.* Van Nostrand Reinhold.

Jacobs G. K., Kerrick D. M., and Krupka K. M. (1981) The high-temperature heat capacity of natural calcite ($CaCO_3$). *Phys. Chem. Minerals* **7,** 55–59.

Kieffer S. W. (1979) Thermodynamics and lattice vibrations of minerals. 3. Lattice dynamics and an approximation for minerals with application to simple substances and framework silicates. *Rev. Geophys. Space Phys.* **17,** 35–59.

Kieffer S. W. (1982) Thermodynamics and lattice vibrations of minerals. 5. Application to phase equilibria, isotopic fractionation and high-pressure thermodynamic properties. *Rev. Geophys. Space Phys.* **20,** 827–849.

Kobayashi K. (1951) The heat capacities of inorganic substances at high temperatures. Part III-The heat capacity of synthetic calcite (calcium carbonate). *Sci. Rep. Tohoku Univ. I* **35,** 103–110.

Kraft S., Knittle E., and Williams Q. (1991) Carbonate stability in the Earth's mantle: a vibrational spectroscopic study of aragonite and dolomite at high pressures and temperatures. *J. Geophys. Res.* **96,** 17997–18010.

Markgraf S. A. and Reeder R. J. (1985) High-temperature structure refinements of calcite and magnesite. *Amer. Mineral.* **70,** 590–600.

O'Neil J. R., Clayton R. N., and Mayeda T. K. (1969) Oxygen isotope fractionation in divalent metal carbonates. *J. Chem. Phys.* **51,** 5547–5558.

Onomichi M. and Kudo K. (1971) Reflection spectra of calcite in far-infrared region. *J. Phys. Soc. Japan* **31,** 1837.

Plihal M. (1973) Lattice dynamics of crystals of the calcite structure. II-Dispersion curve and phonon densities. *Phys. Stat. Sol. (b)* **56,** 495–506.

Polyakov V. B. and Kharlashina N. N. (1994) Effect of pressure on equilibrium isotopic fractionation. *Geochim. Cosmochim. Acta* **58,** 4739–4750.

Reynard B. and Guyot F. (1994) High-temperature properties of geikielite ($MgTiO_3$ ilmenite from high-temperature high-pressure Raman spectroscopy. Some implications for $MgSiO_3$-ilmenite. *Phys. Chem. Mineral.* **21,** 441–450.

Robie R. A. and Edwards J. L. (1966) Some Debye temperatures from single crystal elastic constant data. *J. Appl. Phys.* **37,** 2659–2663.

Sakurai T. and Sato T. (1971) Temperature dependence of vibrational spectra in calcite by means of emissivity measurement. *Phys. Rev.* 583–591.

Salje E. and Viswanathan K. (1976) The phase diagram calcite-aragonite as derived from crystallographic properties. *Contrib. Mineral. Petrol.* **55,** 55–67.

Staveley L. A. K. and Linford R. G. (1969) The heat capacity and entropy of calcite and aragonite, and their interpretation. *J. Chem. Thermodyn.* **1,** 1–11.

Usdowski E. D., Michaelis J., Böttcher M. E., and Hoefs J. (1991) Factors for the oxygen isotope equilibrium between aqueous and gazeous CO_2, carbonic acid, bicarbonate, carbonate, and water (19°C). *Z. Phys. Chem.* **170,** 237–249.

White W. B. (1974) The carbonate minerals. In *The Infrared Spectra of Minerals* (ed. V. C. Farmer), pp. 87–110. Mineral. Soc. Amer.

APPENDIX

Following Guyot et al. (1995) the vibrational Helmoltz free energy F of a crystal can be written

$$F_{vib} = \int \left[\frac{h\nu_i}{2} + k_B T \ln\left(1 - \exp\left(-\frac{h\nu_i}{k_B T}\right)\right) + a_i k_B T^2 \right] g(\nu_i) d\nu_i, \quad (A1)$$

where the summation is over the entire density of states corresponding to 3N oscillators. k_b is the Boltzmann constant. a_i is an intrinsic anharmonic parameter for the ν_i frequency. It is defined by Gillet et al. (1989):

$$a_i = \left(\frac{\partial \ln \nu_i}{\partial T}\right)_V = \alpha(\gamma_{iT} - \gamma_{iP}), \quad (A2)$$

where

$$\gamma_{iT} = K_T \left(\frac{\partial \ln \nu_i}{\partial P}\right)_T, \quad (A3)$$

is the classical mode Grüneisen parameter, and

$$\gamma_{iT} = -\frac{1}{\alpha}\left(\frac{\partial \ln \nu_i}{\partial T}\right)_P, \quad (A4)$$

the mode Grüneisen parameter at constant pressure. K_T is the isothermal bulk modulus and α the coefficient of thermal expansion.

When $a_i = 0$, the oscillators behave as fully harmonic or quasi-harmonic ones. It has been shown that introduction of these parameters in vibrational modelling of C_V accounts for observed deviations from the Dulong and Petit limit at high temperatures (Gillet et al., 1989, 1991). Measuring a_i requires a knowledge of the pressure

and temperature shifts of the vibrational frequencies as well as the incompressibility and thermal expansion of the material. In the absence of Raman and IR data at simultaneous high pressures and temperatures, the volume, dependence of the a_i parameters can be approximated by

$$\left(\frac{\partial \ln a_i}{\partial \ln V}\right)_T = m_i, \quad \text{(A5)}$$

where γ_{iT} is the mode Grüneisen parameter and m_i a parameter yet beyond the capabilities of experimental measurements (Guyot et al., 1996). In the calculations carried in this paper we take $m_i = 0$. The mode Grüneisen parameter γ_{iT} is volume-dependent through relation (A6), defining the parameter q:

$$q_i = \left(\frac{\partial \ln \gamma_{iT}}{\partial \ln V}\right)_T. \quad \text{(A6)}$$

Assuming an entirely vibrational origin for entropy (S) and isochoric specific heat (C_V), they can be deduced from the vibrational Helmholtz free energy by using

$$S = -\left(\frac{\partial F_{vib}}{\partial T}\right)_V,$$

$$S = \int \left[\left(-k_B \ln\left(1 - \exp\left(\frac{-h\nu_i}{k_B T}\right)\right) + \frac{h\nu_i}{T\left(\exp\left(\frac{h\nu_i}{k_B T}\right) - 1\right)} - 2a_i k_B T\right)\right] g(\nu_i) d\nu_i, \quad \text{(A7)}$$

$$C_V = -T\left(\frac{\partial^2 F_{vib}}{\partial T^2}\right)_V,$$

$$C_V = \int \left[\frac{kT\left(\frac{h\nu_i}{k_B T}\right)^2 \exp\left(\frac{h\nu_i}{k_B T}\right)}{\left(\exp\left(\frac{h\nu_i}{k_B T}\right) - 1\right)^2} - 2a_i kT\right] g(\nu_i) d\nu_i. \quad \text{(A8)}$$

The specific heat at constant pressure is obtained from

$$C_P = C_V + \alpha(T)^2 V(T) K_0(T) T, \quad \text{(A9)}$$

where $K_0(T)$ is the bulk modulus at room pressure.

To obtain the volume at simultaneous pressure and temperature we use the Mie-Grüneisen EOS:

$$P = P_{300\,K} + (P_{th} - P_{th\,300\,K}), \quad \text{(A10)}$$

where $P_{300\,K}$ is the static pressure at 300 K, obtained by fitting available experimental room temperature compression data to a third order Birch Murnaghan EOS:

$$P_{300\,K} = \frac{3}{2} K_0 \left[\left(\frac{V_0}{V}\right)^{7/3} - \left(\frac{V_0}{V}\right)^{5/3}\right] \times \left[1 + \frac{3}{4}(K_0' - 4)\left(\left(\frac{V_0}{V}\right)^{2/3} - 1\right)\right]. \quad \text{(A11)}$$

P_{th} and $P_{th\,300\,K}$ represent the thermal pressure at a given pressure and temperature and the thermal pressure at 300 K, respectively. For calcite we took $K_0 = 72$ GPa and $K_0' = 5.37$ (Fiquet et al., 1994). P_{th} is calculated by

$$P_{th} = -\left(\frac{\partial F_{vib}}{\partial V}\right)_T,$$

$$P_{th} = \int \left[\frac{\gamma_i}{V}\left(\frac{h\nu_i}{2} + \frac{h\nu_i}{\left[\exp\left(\frac{h\nu_i}{k_B T}\right) - 1\right]}\right) - \frac{m_i a_i k T^2}{V}\right] g(\nu_i) d\nu_i. \quad \text{(A12)}$$

From the obtained values of $V(P, T)$ one can rederive values of α and K_T at various pressure and temperature conditions. If $m_i = 0$, we have only a quasi-harmonic calculation of the thermal pressure and thus of the EOS.